Appl. Chem. Eng., Vol. 27, No. 3, June 2016, 335-341
http://dx.doi.org/10.14478/ace.2016.1028

Communication

지상 및 미소중력 환경에서 물리적 승화법 공정에 미치는 불순물의 영향 분석: 염화제일수은에 대한 응용성

김극태† · 권무현*

한남대학교 화공신소재공학과, *우석대학교 에너지공학과
(2016년 3월 21일 접수, 2016년 3월 29일 심사, 2016년 4월 5일 채택)

Numerical Analysis for Impurity Effects on Diffusive-convection Flow Fields by Physical Vapor Transport under Terrestrial and Microgravity Conditions: Applications to Mercurous Chloride

Geug Tae Kim† and Moo Hyun Kwon*

Department of Advanced Materials and Chemical Engineering, Hannam University, 1646, Yuseong-daero, Yuseong-gu, Daejeon, 34054 Republic of KOREA
**Department of Energy Engineering, Woosuk University, 66, Daehak-ro, Jincheon-eup, Jincheon-gun Chungcheongbuk-do, 27841 Republic of Korea*
(Received March 21, 2016; Revised March 29, 2016; Accepted April 5, 2016)

초 록

본 연구에서는 지상 및 미소중력환경하에서 물리적 승화법 공정에서의 확산-대류유동에 미치는 불순물의 영향을 이론적으로 Hg_2Cl_2-I_2 시스템에 적용하여 규명하는 것이다. 이론적 해석은 증기상에서 확산-대류 흐름, 열 및 물질전달을 속도 벡터 흐름, 유선, 온도, 농도 분포를 통하여 제시된다. 결정 영역에서의 전체 몰플럭스는 중력가속도와 성분 I_2, 불순물에 상당히 민감하게 반응한다. 성분 I_2을 증가시켰을 때, 농도 대류효과는 확산-대류 유동흐름을 안정화시키는 경향이 있다. 지상중력가속도의 0.001환경에서는 유동흐름은 1차원포물선의 흐름 구조를 나타내며, 확산지배형태를 보여주고 있다. 10^{-3}지상중력가속도 이하에서는 대류 영향은 무시할 수 있다.

Abstract

In this study, impurity effects on diffusive-convection flow fields by physical vapor transport under terrestrial and microgravity conditions were numerically analyzed for the mixture of Hg_2Cl_2-I_2 system. The numerical analysis provides the essence of diffusive-convection flow as well as heat and mass transfer in the vapor phase during the physical vapor transport through velocity vector flow fields, streamlines, temperature, and concentration profiles. The total molar fluxes at the crystal regions were found to be much more sensitive to both the gravitational acceleration and the partial pressure of component I_2 as an impurity. Our results showed that the solutal effect tended to stabilize the diffusive-convection flow with increasing the partial pressure of component I_2. Under microgravity conditions below $10^{-3}g_0$, the flow fields showed a one-dimensional parabolic flow structure indicating a diffusion-dominant mode. In other words, at the gravitational levels less than $10^{-3}g_0$, the effects of convection would be negligible.

Keywords: *microgravity, crystal growth*

1. Introduction

Over the past 45 years since the results of the Apollo space flights, many researches on the role of gravity as a major parameter in materials science and engineering, crystal growth have been extensively carried out in the United States, Russia, Germany, and Japan etc. In particular, through the International Space Station (ISS), various experiments have been carried out based on the American Skylab or Spacelab missions, the German D1 and D2 missions, the Russian Mir station of Foton flights, the European Eureca mission, or the German and the Japanese sounding rocket programs[1]. Fontana *et al.*[2] had investigated crystal growth of sodium chloride in both terrestrial and microgravity environments on the ISS. Single crystal growth diffraction

† Corresponding Author: Hannam University,
Department of Advanced Materials and Chemical Engineering, 1646, Yuseong-daero, Yuseong-gu, Daejeon, 34054 Republic of KOREA
Tel: +82-42-629-8837 e-mail: geugtaekim@gmail.com

pISSN: 1225-0112 eISSN: 2288-4505

shows no change in crystalline structure and cell parameters of NaCl in crystals grown under the microgravity condition of $10^{-6}g_0$, where g_0 denotes the Earth's gravitational acceleration of 981 cm s^{-2}. In 2014, Japanese researchers of Nobeoka *et al*.[3] have reported the numerical simulations of InGaSb crystal growth crystal growth by temperature gradient method on board at the ISS to get a complete understanding for the transport phenomena occurring in the melt system, i.e., in the microgravity fields. Kinoshita *et al*.[4] have grown a silicon germanium alloy crystal $Si_{0.5}Ge_{0.5}$ with 10 mm in diameter by traveling liquidus-zone method in microgravity. Abe *et al*.[5] have studied the numerical simulations of SiGe crystal growth by traveling liquidus-zone method under the microgravity environments. In recent years, many studies on numerical simulations have been carried out under microgravity conditions in various countries[6-18]. In particular, Konishi and Mudawar[19] reported reviews of flow boiling and critical heat flus in microgravity. Carotenuto[20] addressed reviews and relevant results on crystal growth from the vapour phase under microgravity environments, which would be contributed to future microgravity research on board the International Space Station. Yeckel and Derby[21] had investigated the g-jitter (transient acceleration) with steady magnetic fields in vertical Bridgman crystal growth system whose results were relevant to dynamics of three-dimensional convection in microgravity crystal growth. For transverse jitter at intermediate frequencies, flow oscillations were found to be increased, considering in most cases, application of a magnetic field suppresses flow oscillations. Zeng *et al*.[22] investigated three-dimensional oscillatory Marangoni convection in silicone oil liquid bridge under microgravity environments and provided temperature contour lines and projected velocity vector for the range of Marangoni number, from 2.0×10^4 up to 5.0×10^4. Maekawa *et al*.[23] studied the possibility of growing a uniform binary compound crystal in space for InAs-GaAs binary semiconductor by the Bridgman and zone methods. The solution-crystal interface was found to be deformed by buoyancy driven convection in the case of the Bridgman method even in the gravitational acceleration of $10^{-6}g_0$ which is supposed to be the gravity level in the International Space Station. Liu *et al*.[24] carried out simulation of directional solidification or refined Al-7 wt% Si Alloys with comparison with benchmark microgravity experiments.

In general, the crystal growth method by physical vapor transport (PVT) is referred to as a mechanism of sublimation-condensation. The source component-bearing species are vaporized from the source material and recrystallized on a seed crystal, in closed silica glass ampoules in temperature gradient imposed between the source material and the growing crystal. With regard to studies on the PVT in the vapor phase, recently Tebbe *et al*.[25] extended for transition to chaos flow fields in specialty materials of mercurous chloride in applications of microgravity experiments. They have addressed the underlying phenomena in the PVT processes on the relative importance and influencing parameters of diffusion-advection, thermal and/or solutal convection on mass transport. It is reported that Hg_2Cl_2 single crystals have applications for acousto-optic and opto-electronic devices such as Bragg cells, X-ray detectors operating at ambient temperatures[26]. In study we employ a material of Hg_2Cl_2 as a model sample and investigate numerically the influence of

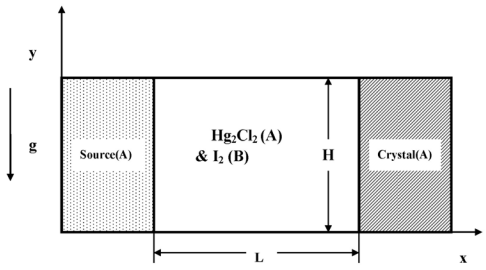

Figure 1. Schematic description of a two-dimensional PVT model for a Hg_2Cl_2-I_2 system.

gravitational accelerations on diffusive convection during the PVT of a mixture of Hg_2Cl_2 vapor and impurity of I_2. The distinction of this study in a comparison with our previous study[27-28] is centered into the effects of gravitational accelerations and the partial pressure of component I_2 with high molecular weight through numerical simulations of vector, streamline, temperature and concentration profiles.

2. Numerical Analysis

A physical model is created with a two-dimensional rectangular enclosure with aspect ratio (transport length L to height H) of 5, as shown in Figure 1. The source is maintained at a temperature T_s, while the growing crystal is at a temperature T_c, with $T_s > T_c$. PVT of the transported component A (Hg_2Cl_2) occurs inevitably, due to presence of impurity, i.e., a component B (I_2). The transport of fluid within a rectangular PVT crystal growth reactor is governed by a system of elliptic, coupled conservation equations for mass (continuity), momentum, energy and species (diffusion), Eq. (1) with appropriate boundary conditions, Eqs. (2)-(4), which can be found in Refs.[27-29]. The density of the vapor mixture of component A (Hg_2Cl_2) and B (I_2) is assumed constant except the buoyancy body force term, which would be a function of both temperature and concentration.

$$\nabla \bullet (\rho u \phi) = \nabla \bullet (\Gamma \nabla \phi) + S \tag{1}$$

On the walls ($0 < x^* < L/H$, $y^* = 0$ and 1) :

$$u^*(x^*,0) = u^*(x^*,1) = v^*(x^*0) = v^*(x^*,1) = 0 \tag{2}$$
$$\frac{\partial \omega_A^*(x^*,0)}{\partial y^*} = \frac{\partial \omega_A^*(x^*,1)}{\partial y^*} = 0,$$
$$T^*(x^*,0) = T^*(x^*,1) = \frac{T - T_c}{T_s - T_c}$$

On the source ($x^* = 0$, $0 < y^* < 1$) :

$$u^*(0,y^*) = -\frac{1}{Le}\frac{\Delta\omega}{(1-\omega_{A,s})}\frac{\partial \omega_A^*(0,y^*)}{\partial x^*} \tag{3}$$
$$v^*(0,y^*) = 0,$$
$$T^*(0,y^*) = 1,$$
$$\omega_A^*(0,y^*) = 1.$$

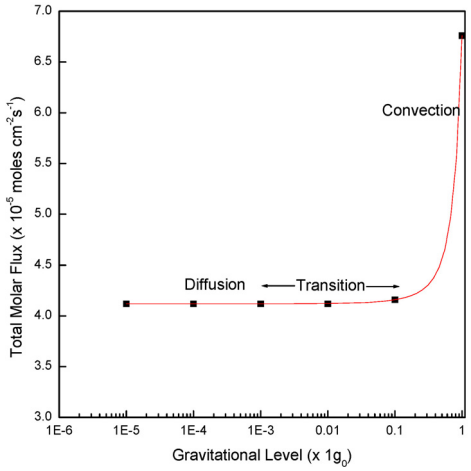

Figure 2. Effects of gravitational levels on the total molar flux for various gravitational accelerations, $10^{-5}g_0 \le g \le 1g_0$, in the negative y-direction, where g0 denotes the Earth's gravitational acceleration of 981 cm s^{-2}. Based on aspect ratio = 5 (L = 10 cm), a linear wall temperature profile between T_s = 623.5 K and T_c = 563.15 K.

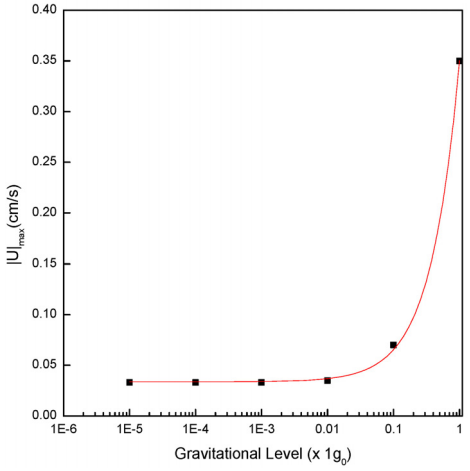

Figure 3. Effects of gravitational levels on $|U|_{max}$ for various gravitational accelerations, $10^{-5}g_0 \le g \le 1g_0$, corresponding to Figure 2.

On the crystal ($x^* = L/H$, $0 < y^* < 1$) :

$$u^*(L/H, y^*) = -\frac{1}{Le}\frac{\Delta\omega}{(1-\omega_{A,c})}\frac{\partial\omega_A^*(L/H, y^*)}{\partial x^*} \quad (4)$$

$$v^*(L/H, y^*) = 0,$$

$$T^*(L/H, y^*) = 0,$$

$$\omega_A^*(L/H, y^*) = 0.$$

3. Results and Discussion

The purpose of this research is to perform the numerical analysis of the influence of impurity and gravitational levels on diffusive-convection flow fields by the PVT of Hg_2Cl_2 with impurity of I_2, from a point of view of the total mass flux and interfacial distributions. Because the molecular weight of an impurity (I_2) is not equal to that of the crystal component (Hg_2Cl_2) during the physical vapor transport, both thermal and/or solutal convection always occur and also become much important in mass transport. In this study, a linear temperature profile at the walls is chosen. Detailed data such as typical process parameters and physical properties for the operating conditions could be found in Refs.[27-29].

Figure 2 shows our numerical results for the effects of gravitational levels on the total molar flux for various gravitational accelerations, $10^{-5}g_0 \le g \le 1g_0$, in the negative y-direction, where g_0 denotes the Earth's gravitational acceleration of 981 cm s^{-2}. The convection is predominant over the diffusion for the range from $1g_0$ down to $0.1g_0$. The total molar flux is sharply decreased with decreasing the gravitational level from $1g_0$ down to $0.1g_0$. From a point of view of the total mass flux, the transition from the convection to the diffusion mode occurs in the range of $10^{-2}g_0 \le g \le 0.1g_0$, and reflects the diffusion-convection mode. There is little difference of the total mass flux between $0.1g_0$ and $10^{-2}g_0$. The total molar flux in a convection region of $1g_0$ is greater than in the diffusion region of $10^{-2}g_0$ by a factor of 1.6. It should be noted that the flow fields under terrestrial conditions include both the convection and diffusion, but the convection is predominant over the diffusion.

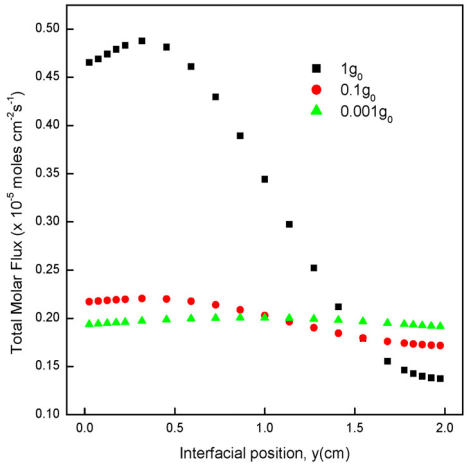

Figure 4. Interfacial distributions of the total molar flux for three different gravitational levels, $1g_0$, $0.1g_0$ and $10^{-3}g_0$.

Figure 3 shows the effects of gravitational levels on $|U|_{max}$ for various gravitational accelerations, $10^{-5}g_0 \le g \le 1g_0$, corresponding to Figure 2. The $|U|_{max}$ denotes the dimensional maximum magnitude of velocity vector in the vapor phase, and reflects the intensity of convection in the vapor phase during the physical vapor transport of Hg_2Cl_2 with impurity of I_2. As the gravitational level is decreased from $1g_0$ down to $0.1g_0$, the $|U|_{max}$ under the condition of $0.1g_0$ is reduced to one-fifth of the $|U|_{max}$ under the condition of $1g_0$. With decreasing the gravitational level from $0.1g_0$ down to $10^{-2}g_0$, the $|U|_{max}$ under the condition of $10^{-2}g_0$ leads to one half of the $|U|_{max}$ under the condition of $0.1g_0$. Considering little difference of total mass flux between $0.1g_0$ and $10^{-2}g_0$ previously, from a point of view of dimensional maximum magnitude of velocity vector, the transition from the convection to the diffusion mode occurs in the range of $10^{-3}g_0 \le g \le 0.1g_0$. From Figures 3 and 4, it is concluded that the transition from the convection

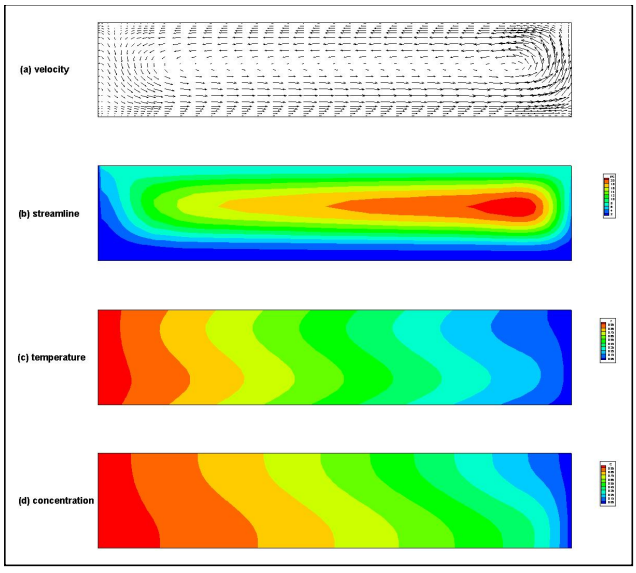

Figure 5. (a) velocity, (b) streamline ($\triangle\psi$ = 2, ψ_{max} = 21.71, ψ_{min} = 2), (c) temperature ($\triangle T$ = 0.1, T_{max} = 1.0, T_{min} = 0), (d) concentration ($\triangle C$ = 0.1, C_{max} = 1.0, C_{min} = 0), based on aspect ratio = 5, $\triangle T$ = 60 K (623.15 K → 563.15 K), and $1g_0$. A relative velocity vector with a magnitude of 100 has 1.4 cm. The maximum velocity vector is 0.35 cm s^{-1}.

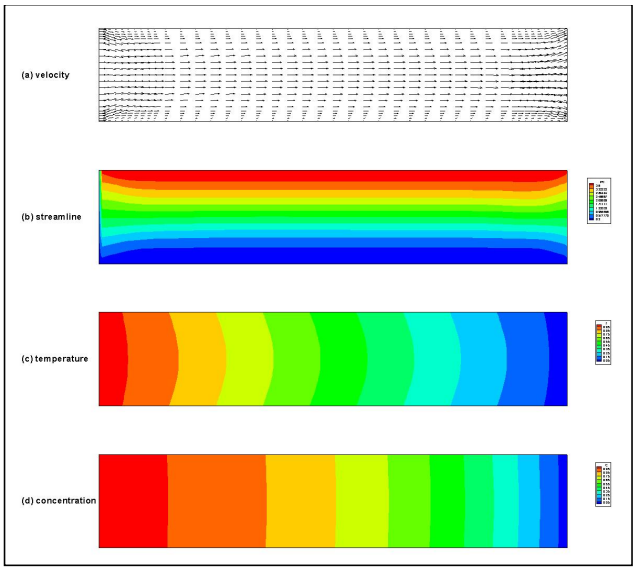

Figure 6. (a) velocity, (b) streamline ($\triangle\psi$ = 0.37, ψ_{max} = 3.6, ψ_{min} = 0.2), (c) temperature ($\triangle T$ = 0.1, T_{max} = 1.0, T_{min} = 0), (d) concentration ($\triangle C$ = 0.1, C_{max} = 1.0, C_{min} = 0), based on aspect ratio = 5, $\triangle T$ = 60 K (623.15 K → 563.15 K), and $10^{-3}g_0$. A relative velocity vector with a magnitude of 100 has 1 cm. The maximum velocity vector is 0.033 cm s^{-1}.

to the diffusion mode occurs in the range of $10^{-3}g_0 \leq g \leq 0.1g_0$.

Figure 4 shows the interfacial distributions of the total molar flux for three different gravitational levels, $1g_0$, $0.1g_0$ and $10^{-3}g_0$. The case of $1g_0$ shows the convective flow indicates asymmetrical at the position of y = 1 cm and three dimensional flow structure. The case of $0.1g_0$ is also likely to be slightly asymmetrical at the position of y = 1 cm and three dimensional flow structure. It is clear that the profiles of the total molar flux against the interfacial position are symmetrical at the position of y = 1 cm and nearly flat. The deviations of maximum and minimum total molar flux from the average total molar flux for $0.1g_0$ and $10^{-3}g_0$ are much smaller than for $1g_0$.

The mass transport phenomena occurring in the vapor phase when growing single crystals of Hg_2Cl_2 by the method of vapor crystal growth under terrestrial and microgravity environments are numerically investigated. By examining plots of the distributions of vector and stream function, and temperature and concentration, an appreciation for the nature of the diffusive-convection and/or diffusive flow and the temperature, and the concentration fields can be obtained. Figures 5 and 6 show (a) velocity, (b) streamline, (c) temperature, (d) concentration field, based on Ar = 5, △T = 60 K (623.15 K → 563.15 K), corresponding to $1g_0$, and $10^{-3}g_0$, respectively. In Figure 5, a relative velocity vector with a magnitude of 100 has 1.4 cm and the maximum velocity vector is 0.35 cm s^{-1}, whereas in Figure 6, a relative velocity vector with a magnitude of 100 has 1 cm and the maximum velocity vector is 0.033 cm s^{-1}. As shown in Figure 5, all fields (5(a)-5(d)) are asymmetrical about the centerline axis of y = 1 cm and exhibit a three dimensional flow structure with one single cell in the vapor phase. To study the effects of gravitational acceleration on flow fields of vector, stream function, temperature and concentration, a $10^{-3}g_0$ of microgravity acceleration is chosen, under whose condition it would increase the diffusive flow and yield one-dimensional parabolic flow pattern in the vapor phase. This indicates thermal and/or solutal buoyancy driven convection is very weak under $10^{-3}g_0$ of microgravity, it is impossible for the effect of buoyancy force to contribute significantly to heat and/or mass transport. Thus, our results at the $10^{-3}g_0$ of microgravity show that both temperature and concentration gradients become uniform near the crystal region, which is an ideal growth condition for the high quality of crystal. For the simulations shown in Figures 5 and 6, we choose a field strength of P_B = 100 Torr for the cases considered here.

As shown in Figure 5(a), the magnitudes of velocity vector near the crystal region are shown to be greater than those near the source interface. The magnitudes of velocity vector in the lower half region are nearly same those in the upper half region along the centerline, dimensional y = 1 cm, which indicates a strong convective structure under operating conditions of △T = 60 K (623.15 K → 563.15 K), and $1g_0$, P_B = 100 Torr, aspect ratio (transport length-to-width) = 5.0, Prandtl number = 1.1, Lewis number = 0.7, thermal Grashof number = 1.0×10^5, solutal Grashof number = 4.7×10^5, thermal diffusivity of 0.07 cm^2s^{-1}, kinematic viscosity of 0.08 cm^2s^{-1}, binary diffusivity of 0.10 cm^2s^{-1}. The temperature profile along the centerline of dimensional y = 1 cm exhibits a cosine wave curve, indicating a uniform imposed temperature profile on ampoule walls. As shown in Figure 5(d), with regards to concentration profile, the concentrations in front of the source interface are relatively uniform, and significantly varied near the crystal interface. As shown in Figure 6, all fields (6(a)-6(d)) are symmetrical about the centerline axis of y = 1 cm and exhibit a one-dimensional flow structure, diffusion-dominant in comparison with the

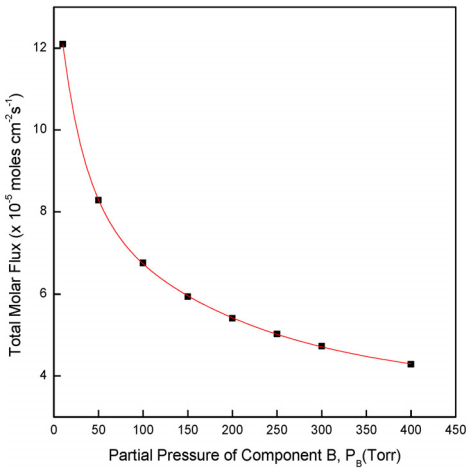

Figure 7. Effects of partial pressure of component B, P_B(Torr) on the total molar flux for various partial pressure of component B, P_B, 10 ≤ P_B(Torr) ≤ 400.

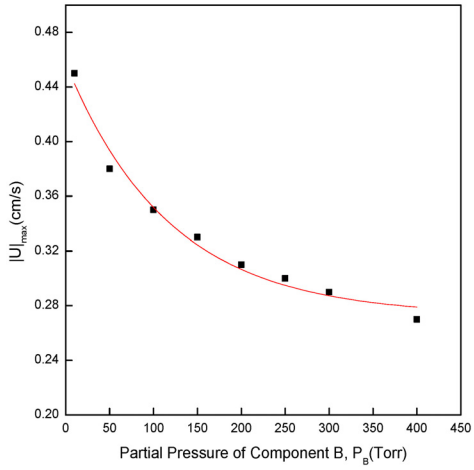

Figure 8. Effects of partial pressure of component B, P_B(Torr) on $|U|_{max}$ for various partial pressure of component B, P_B, 10 ≤ P_B(Torr) ≤ 400, corresponding to Figure 7.

effect of convection.

One of the practical methods for controlling the crystal growth rate is to increase the partial pressure of the component B as an impurity. Thus, we investigate the influences of the impurity on diffusive-convection flow fields by physical vapor transport. Figure 7 shows the effects of partial pressure of component B, P_B on the total molar flux for various partial pressure of component B, 10 ≤ P_B(Torr) ≤ 400. The total molar flux decays second-order exponentially with increasing the partial pressure of component B, for 10 ≤ P_B(Torr) ≤ 400. For 10 ≤ P_B(Torr) ≤ 100, the total molar flux falls sharply, and for 10 ≤ P_B(Torr) ≤ 400, the total molar flux is nearly linearly decreased with the partial pressure of component B. The total molar flux at P_B = 10 Torr is nearly doubled than that at P_B = 150 Torr, with decreasing the partial pressure of component B by a factor of one-seventh. Figure 8 shows the effects of partial pressure of component B, P_B(Torr) on $|U|_{max}$ for various partial pressure of component B, P_B, 10 ≤ P_B(Torr) ≤ 400, corresponding to Figure 7. The $|U|_{max}$ decays sec-

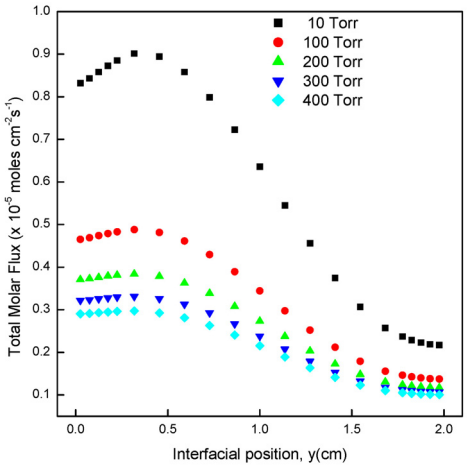

Figure 9. Interfacial distributions of the total molar flux for five partial pressures of component B, P_B(Torr).

ond-order exponentially with increasing the partial pressure of component B, P_B, for 10 ≤ P_B(Torr) ≤ 400. The $|U|_{max}$ decreases with partial pressure of component B, P_B by a gradient of 8.6×10^{-4} cm $s^{-1}Torr^{-1}$ for 10 ≤ P_B(Torr) ≤ 150. The $|U|_{max}$ decreases directly and linearly with partial pressure of component B, P_B by a gradient of 2.4×10^{-4} cm $s^{-1}Torr^{-1}$ for 150 ≤ P_B(Torr) ≤ 400. The gradient in the range of 10 ≤ P_B(Torr) ≤ 150 is found to be 3.58 times than that in the range of 150 ≤ P_B(Torr) ≤ 400.

Figure 9 shows the interfacial distributions of the total molar flux for five partial pressures of component B, P_B to study non-uniformities against the center of y = 1 cm. The convection enhances the overall mass transport of component A (Hg_2Cl_2), and, then results in an increase in its total molar flux, but pays for the expense of uniformity in the total molar flux, with the specific interfacial distribution revealing dominance of diffusive convection. This result is consistent with earlier results[30-31]. The total molar fluxes for all cases under consideration, as shown in Figure 9, imply the occurrence of one cell in front of the crystal region, and the results for P_B = 100 Torr, and $1g_0$ are found to be confirmed, as shown in Figure 3. All profiles of the total molar flux against dimensional interfacial position are asymmetric against the center position of y = 1 cm. Moreover, the maximum value of the total molar flux for all cases occurs between y = 0 cm and y = 0.5 cm, the maximum value of the total molar flux for the case of P_B = 10 Torr is about twice that for P_B = 100 Torr. It should be noted that fluid is assumed to cling to solid surfaces, i.e., walls with which it is in contact. In other words, the velocities of the mixture of vapor A and B at walls, i.e., y = 0 cm and 2 cm, are assumed to be zero. As shown in Figures 7 through 9, our results have indicated that by increasing the partial pressure of component B, the solutal effect is found to have the stabilizing effect of diffusive-convection flow and, thus, the maximum total molar flux near at y = 0.5 cm is decreased.

4. Conclusions

For the study of the influences of impurity on diffusive-convection flow fields by physical vapor transport of Hg_2Cl_2 under terrestrial and microgravity conditions, we carried out numerical simulations. It is concluded that the diffusive convection flow fields, total molar flux at the crystal regions are much sensitive to the gravitational accelerations, partial pressure of component of B. Under microgravity conditions below $10^{-3}g_0$, the flow fields are found to be a one-dimensional parabolic flow structure which implies a diffusion-dominant mode. For the convection region of $10^{-1}g_0 \leq g \leq 1g_0$, one cell in the vapor phase occurs for all cases under consideration of the total molar fluxes for $10 \leq P_B(\text{Torr}) \leq 400$. Also, at the gravitational level of $10^{-3}g_0$, the effect of convection is likely to be negligible.

Acknowledgement

This research has been financially supported by the Hannam University for support of the current investigations through a one-year professor-yeonguneon program starting from September 1, 2014 (September 1, 2014 to August 31, 2015).

References

1. K. W. Benz and P. Dold, Crystal growth under microgravity: present results and future prospects towards the international space station, *J. Cryst. Growth*, **237-239**, 1638-1645 (2002).
2. P. Fontana, J. Schefer, and D. Pettit, Characterization of sodium chloride crystals grown in microgravity, *J. Cryst. Growth*, **324**, 207-211 (2011).
3. M. Nobeoka, Y. Takagi, Y. Okano, Y. Hayakawa, and S. Dost, Numerical simulation of InGaSb crystal growth by temperature gradient method under normal- and micro-gravity fields, *J. Cryst. Growth*, **385**, 66-71 (2014).
4. K. Kinoshita, Y. Arai, Y. Inatomi, T. Tsukada, S. Adachi, H. Miyata, R. Tanaka, J. Yoshikawa, T. Kihara, H. Tomioka, H. Shibayama, Y. Kubota, Y. Warashina, Y. Sasaki, Y. Ishizuka, Y. Harada, S. Wada, T. Ito, M. Takayanagi, and S. Yoda, Growth of a $Si_{0.50}Ge_{0.50}$ crystal by the traveling liquids-zone (TLZ) method in microgravity, *J. Cryst. Growth*, **388**, 12-16 (2014).
5. K. Abe, S. Sumioka, K.-I. Sugioka, M. Kubo, T. Tsukada, K. Kinoshita, Y. Arai, and Y. Inatomi, Numerical simulation of SiGe crystal growth by the traveling llquidus-zone method in a microgravity environment, *J. Cryst. Growth*, **402**, 71-77 (2014).
6. C. Stelian and T. Duffar, Influence of rotating magnetic fields on THM growth of CdZnTe crystals under microgravity and ground conditions, *J. Cryst. Growth*, **429**, 19-26 (2015).
7. Z. Li, J. H. Peterson, A. Yeckel, and J. J. Derby, Analysis of the effects of a rotating magnetic field on the growth of cadmium zinc telluride by the traveling heater method under microgravity conditions, *J. Cryst. Growth*, Doi: 10.1016/j.jcrysgro.2015.12.046.
8. W. M. B. Duval, N. B. Singh, and M. E. Glicksman, Physical vapor transport of mercurous chloride crystals: design of a microgravity experiment, *J. Cryst. Growth*, **174**, 120-129 (1997).
9. E. N. Kolesnikova, Yu. A. Polovko, V. S. Yuferev, and A. I. Zhmakin, Influence of coriolis force on thermal convection and impurity segregation during crystal growth under microgravity, *J. Cryst. Growth*, **180**, 578-586 (1997).
10. F. Otálora and J. M. García-Ruiz, Crystal growth studies in microgravity with the APCF Ⅰ. Computer simulation of transport dynamics, *J. Cryst. Growth*, **182**, 141-154 (1997).
11. J. M. García-Ruiz and F. Otálora, Crystal growth studies in microgravity with the APCF Ⅱ. Image analysis studies, *J. Cryst. Growth,* **182**, 155-167 (1997).
12. C. W. Lan and C. Y. Tu, Three-dimensional analysis of flow and segregation control by slow rotation for Bridgman crystal growth in microgravity, *J. Cryst. Growth*, **237**, 1881-1885 (2002).
13. S. Maruyama, K. Ohno, A. Komiya, and S. Sakai, Description of the adhesive crystal growth under normal and micro-gravity conditions employing experimental and numerical approaches, *J. Cryst. Growth*, **245**, 278-288 (2002).
14. M. Catauro, F. Bollino, and F. Papale, Response of SAOS-2 cells to simulated microgravity and effect of biocompatible sol-gel hybrid coatings, *Acta Astronaut.*, **122**, 237-242 (2016).
15. K. Harth, T. Trittel, K. May, S. Wegner, and R. Stannarius, Three-dimensional (3D) experimental realization and observation of a granular gas in microgravity, *Adv. Space Res.*, **55**, 1901-1912 (2015).
16. K. Nishino, T. Yano, H. Kawamura, S. Matsumoto, I. Ueno, and M. K. Ermakov, Instability of thermocapillary convection in long liquid bridges of high Prandtl number fluids in microgravity, *J. Cryst. Growth*, **420**, 57-63 (2015).
17. Y. Yang, L. M. Pan, and J.-J. Xu, Effects of microgravity on Marangoni convection and growth characteristic of a single bubble, *Acta Astronaut.*, **100**, 129-139 (2014).
18. D. E. Melinikov, V. Shevtsova, T. Yano, and K. Nishino, Modeling of the experiments on the Marangoni convection in liquid bridges in weightlessness for a wide range of aspect ratios, *Int. J. Heat Mass Transf.*, **87**, 119-127 (2015).
19. C. Konishi and I. Mudawar, Review of flow boiling and critical heat flux in microgravity, *Int. J. Heat Mass Transf.*, **80**, 469-493 (2015).
20. L. Carotenuto, Crystal growth from the vapour phase in microgravity*, Prog. Cryst. Growth Charact. Mater.*, **48/49**, 166-188 (2004).
21. A. Yeckel and J. J. Derby, Dynamics of three-dimensional convection in microgravity crystal growth: G-jitter with steady magnetic fields, *J. Cryst. Growth*, **263**, 40-52 (2004).
22. Z. Zeng, H. Mizuseki, K. Simamura, T. Fukuda, K. Higashino, and Y. Kawazoe, Three-dimensional oscillatory thermocapillary convection in liquid bridge under microgravity, *Int. J. Heat Mass Transf.*, **44**, 3765-3774 (2001).
23. T. Maekawa, Y. Hiraoka, K. Ikegami, and S. Matsumoto, Numerical modelling and analysis of binary compound semiconductor growth under microgravity conditions, *J. Cryst. Growth*, **229**, 605-609 (2001).
24. D. R. Liu, N. Mangelinck-Noël, C. A. Gandin, G. Zimmermann, L. Sturz, H. Nguyen-Thi, and B. Billia, Simulation of directional solidification of refined Al-7wt.% Si alloys – Comparison with benchmark microgravity experiments, *Acta Mater.*, **93**, 24-37 (2015).
25. P. A. Tebbe, S. K. Loyalka, and W. M. B. Duval, Finite element modeling of asymmetric and transient flow fields during physical

vapor transport, *Finite Elem. Anal. Des.*, **40**, 1499-1519 (2004).
26. N. B. Singh, M. Gottlieb, G. B. Brandt, A. M. Stewart, R. Mazelsky, and M. E. Glicksman, Growth and characterization of mercurous halide crystals: mercurous bromide system, *J. Cryst. Growth*, **137**, 155-160 (1994).
27. Y. K. Lee and G. T. Kim, Effects of convection on physical vapor transport of Hg_2Cl_2 in the presence of Kr-Part I: under microgravity environments, *J. Korean Cryst. Growth Cryst. Technol.*, **23**, 20-26 (2013).
28. G. T. Kim, Effects of aspect ratio on diffusive-convection during physical vapor transport of Hg_2Cl_2 with impurity of NO, *Appl. Chem. Eng.*, **26**, 746-752 (2015).
29. G. T. Kim and M. H. Kwon, Effects of solutally dominant convection on physical vapor transport for a mixture of Hg_2Br_2 and Br_2 under microgravity environments, *Korean Chem. Eng. Res.*, **52**, 75-80 (2014).
30. D. W. Greenwell, B. L. Markham, and F. Rosenberger, Numerical modeling of diffusive physical vapor transport in cylindrical Ampoules, *J. Cryst. Growth*, **51**, 413-425 (1981).
31. B. L. Markham, D. W. Greenwell, and F. Rosenberger, Numerical modeling of diffusive-convective physical vapor transport in cylindrical vertical ampoules, *J. Cryst. Growth*, **51**, 426-437 (1981).